

SUPPORTING INFORMATION

Ultrafast dynamics in LMCT and intraconfigurational excited states in hexahaloiridates(IV), models for heavy transition metal complexes and building blocks of quantum correlated materials

Darya S. Budkina,^{a,b} Firew T. Gemedo,^a Sergey M. Matveev,^{a,c} and Alexander N. Tarnovsky^{a†}

^a Department of Chemistry and Center for Photochemical Sciences, Bowling Green State University, Bowling Green, OH, 43402, USA

^b Present address: School of Chemistry and Biochemistry, University of Geneva, 1211 Geneva 4, Switzerland

^c Present address: Department of Chemistry, University of Illinois at Urbana-Champaign, Champaign-Urbana, Illinois 61801, USA

† E-mail: atarnov@bgsu.edu.

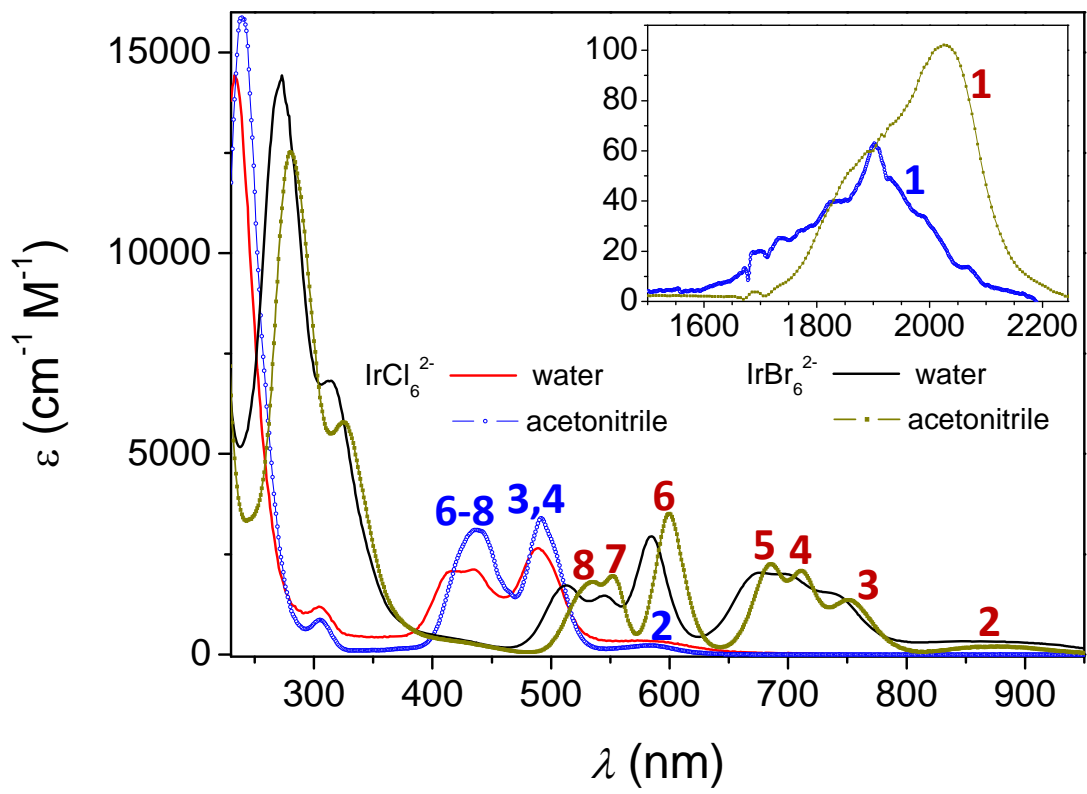


Figure S1. The comparison of the steady-state absorption spectra (extinction coefficient, ε) of IrCl_6^{2-} and IrBr_6^{2-} in acetonitrile and water. The inset shows the $E_g'' \rightarrow U_g'$ intraconfigurational absorption band for IrCl_6^{2-} (blue open symbols) and IrBr_6^{2-} (dark yellow solid symbols) in acetonitrile. Electronic transitions of IrCl_6^{2-} and IrBr_6^{2-} are numbered 1-8 for spectral assignments; see Table 1 in the main text.

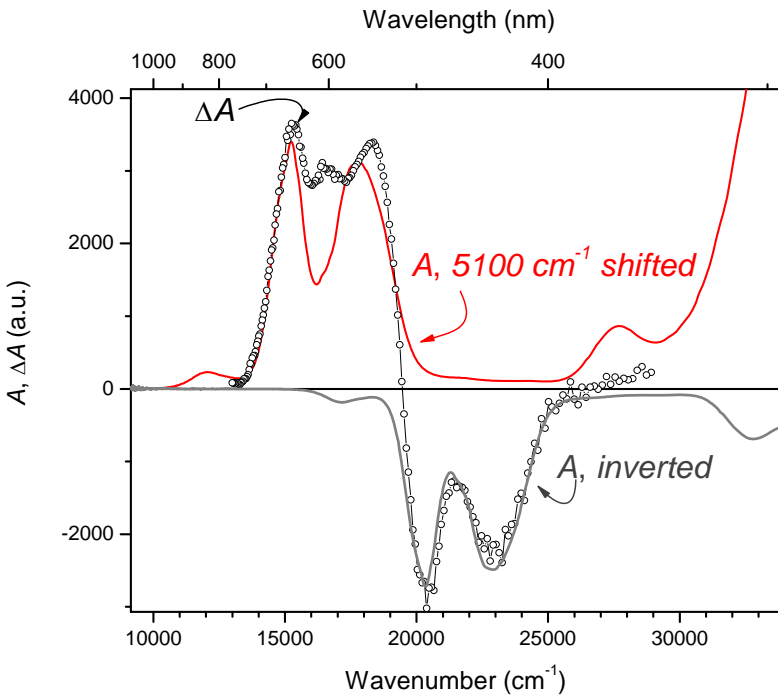


Figure S2. IrCl_6^{2-} in acetonitrile: the positions of two intense 655- and 544-nm ΔA bands (20 ps, 600-nm excitation) match the positions of the ~ 492 and ~ 437 nm steady-state absorption bands when the steady-state spectrum is shifted (red line) by the energy gap (5100 cm^{-1}) between the ground and the first-excited intraconfigurational states. This suggests that the 655 and 544 nm bands are due to ESA from the intraconfigurational state into the same excited states reached upon 492 and 437 nm transitions from the ground state. The grey line depicts the steady-state absorption spectrum of IrCl_6^{2-} in acetonitrile, which when inverted and scaled to the ground-state bleach in the 20 ps ΔA spectrum, is superimposable with the latter. This suggests that ground-state bleach predominates over ESA within the region of negative ΔA signals. Because ground-state bleach exhibits only minor spectral changes from the shortest to the longest delay times at all excitation wavelengths studied, one can conclude that ΔA signals within the ground-state bleach region report exclusively on the repopulation of the ground electronic state and are not sensitive to the population transitions between the excited states.

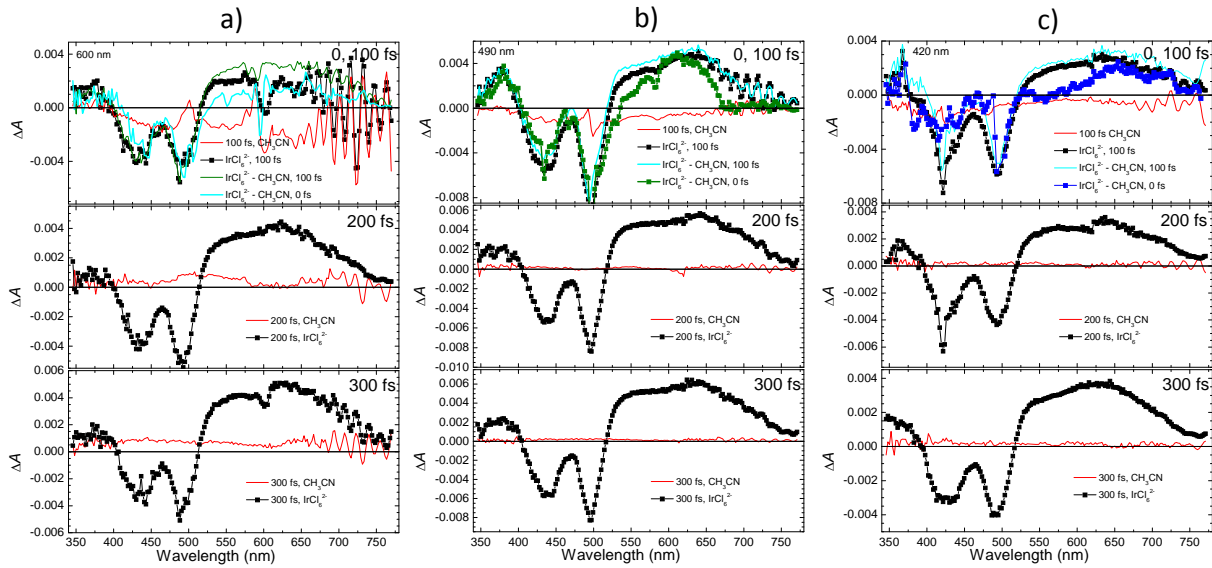


Figure S3. The comparison of short-time (0–300 fs) ΔA signals for IrCl_6^{2-} in acetonitrile solutions and neat acetonitrile measured under identical conditions following excitation at 600 nm (a), 490 nm (b), and 420 nm (c). The 0 (not shown) and 100 fs (shown as lines) ΔA signals of neat CH_3CN were scaled to account for the solute absorbance at a given excitation wavelength and subtracted from the solution ΔA data. The top panels show the resulting 0 and 100 fs ΔA spectra, where the 100 fs spectra (shown before and after the subtraction) illustrate the effect of the subtraction. The acetonitrile ΔA signals at 200 and 300 fs (lines) were much smaller than the corresponding ΔA signals from the solution (symbols), so that the solvent contribution at these delay times was concluded to be negligibly small. For delay times longer than 300 fs, the 600, 490, and 420 nm excitation of neat acetonitrile yielded zero ΔA signals.

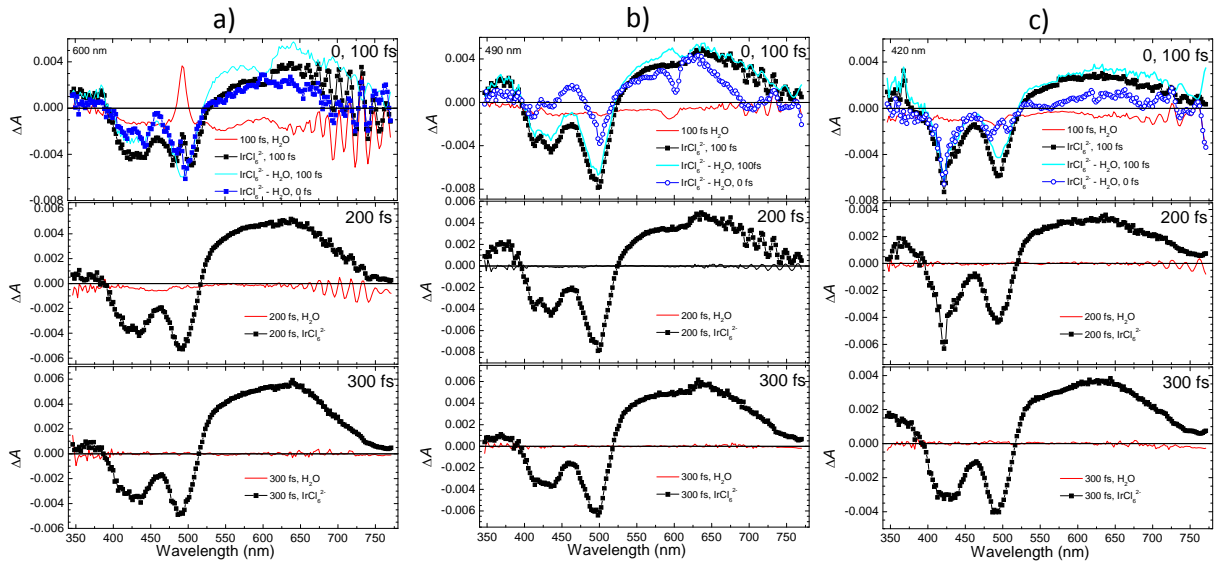


Figure S4. The comparison of short-time ΔA signals for aqueous IrCl_6^{2-} and neat water measured under identical conditions following excitation at 600 nm (a), 490 nm (b), and 420 nm (c). The 0 (not shown) and 100 fs (shown as lines) ΔA signals of neat water were scaled to account for the solute absorbance at a given excitation wavelength and subtracted from the solution ΔA data. The top panels show the resulting 0 and 100 fs ΔA spectra, where the 100 fs spectra (shown before and after the subtraction) illustrate the effect of the subtraction. Because water ΔA signals (lines) were much smaller than the ΔA signals from the solution (symbols) at 200 and 300 fs, the solvent contribution at these delay times was concluded to be negligibly small. For delay times longer than 300 fs, the 600, 490, and 420 nm excitation of neat water yielded zero ΔA signals.

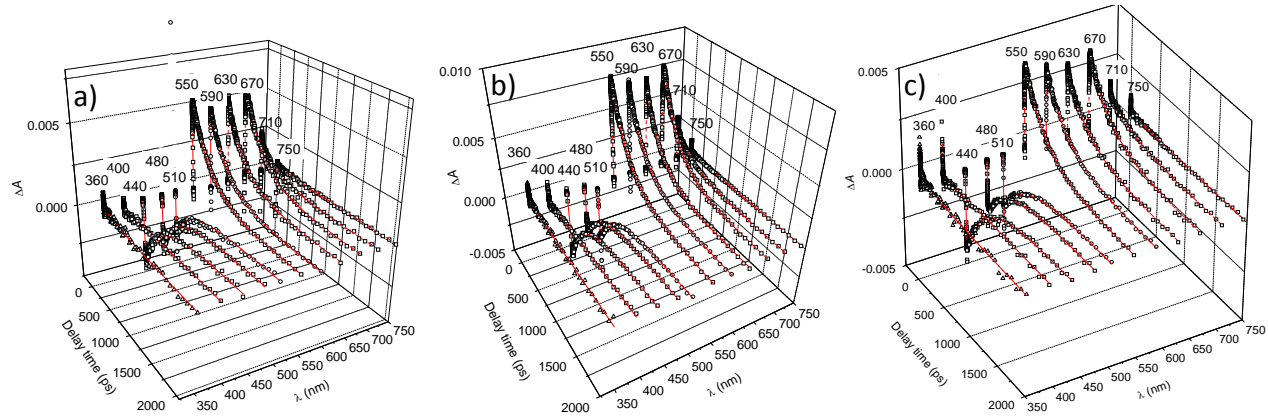


Figure S5. Representative transient absorption kinetic traces (symbols) of IrCl_6^{2-} in acetonitrile following excitation at 600 nm (a), 490 nm (b), and 420 nm (c). The probe wavelengths (nm) are shown besides each kinetic trace. Multiexponential fits resulting from the global analysis described in the main text are shown as solid red lines.

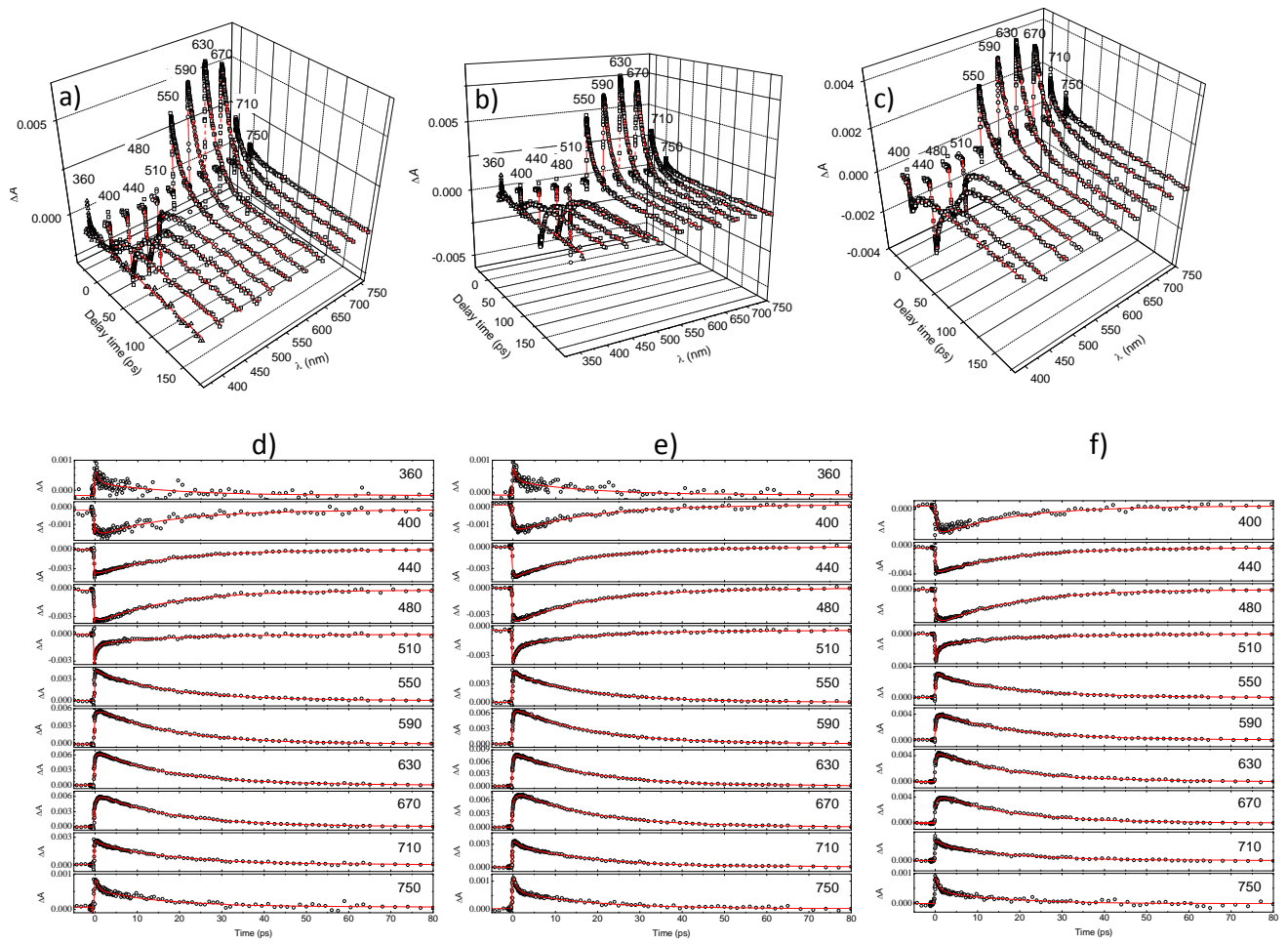


Figure S6. Representative transient absorption kinetic traces (symbols) of aqueous IrCl_6^{2-} following excitation at 600 nm (a), 490 nm (b), and 420 nm (b). The probe wavelengths (nm) are shown besides each kinetic trace. Multiexponential fits resulting from the global analysis as described in the main text are shown as solid red lines. Panels d), e), and f) show conventional two-dimensional plots of transient absorption as a function of the time delay for 600-, 490, and 420-nm excitation, respectively.

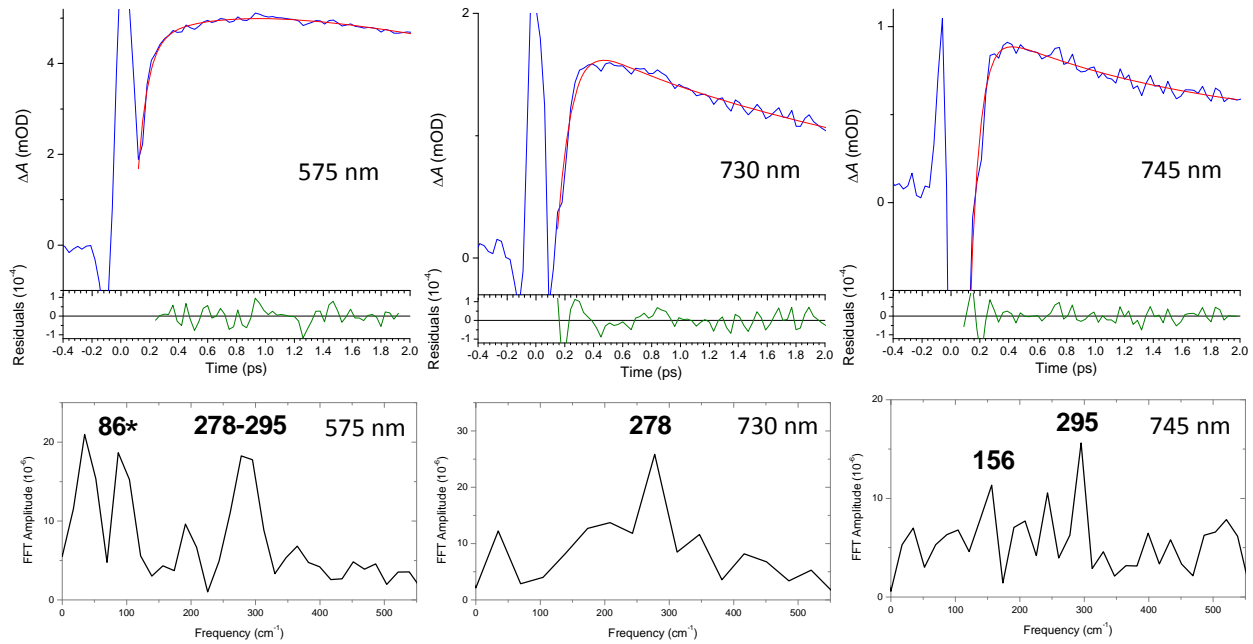


Figure S7a. Aqueous IrCl_6^{2-} , 600-nm excitation: the ΔA kinetic traces at several probe wavelengths (blue), the multiexponential fits (red), and the fit residuals (green). The FFT spectra of the residuals are dominated by the $287 \pm 9 \text{ cm}^{-1}$ band due to the IrCl_6^{2-} ground-state wavepackets induced via ISRS (Raman e_g mode: $290\text{-}293 \text{ cm}^{-1}$, Table S1). An asterisk marks the 86 cm^{-1} FFT band also observed in the flow cell filled with neat water.

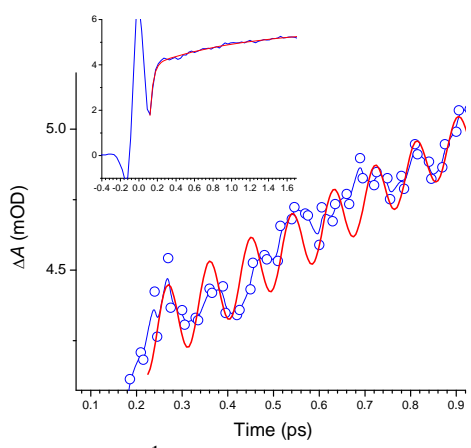


Figure S7b. IrCl_6^{2-} in acetonitrile, 600-nm excitation. The representative 605-nm ΔA kinetic trace illustrates the coherent modulation persisting for about two picoseconds. This oscillation is best modeled by a 350 cm^{-1} frequency (red), which matches the frequency of the a_{1g} Raman-active mode of ground-state IrCl_6^{2-} (345 cm^{-1} , acetonitrile¹), and therefore, is assigned to ground-state wavepackets produced via ISRS. Excitation of this mode is not efficient because of the small bandwidth of the $\sim 70\text{-}75 \text{ fs}$ excitation pulse (220 cm^{-1} , fwhm). Oscillations at lower frequencies were not observed.

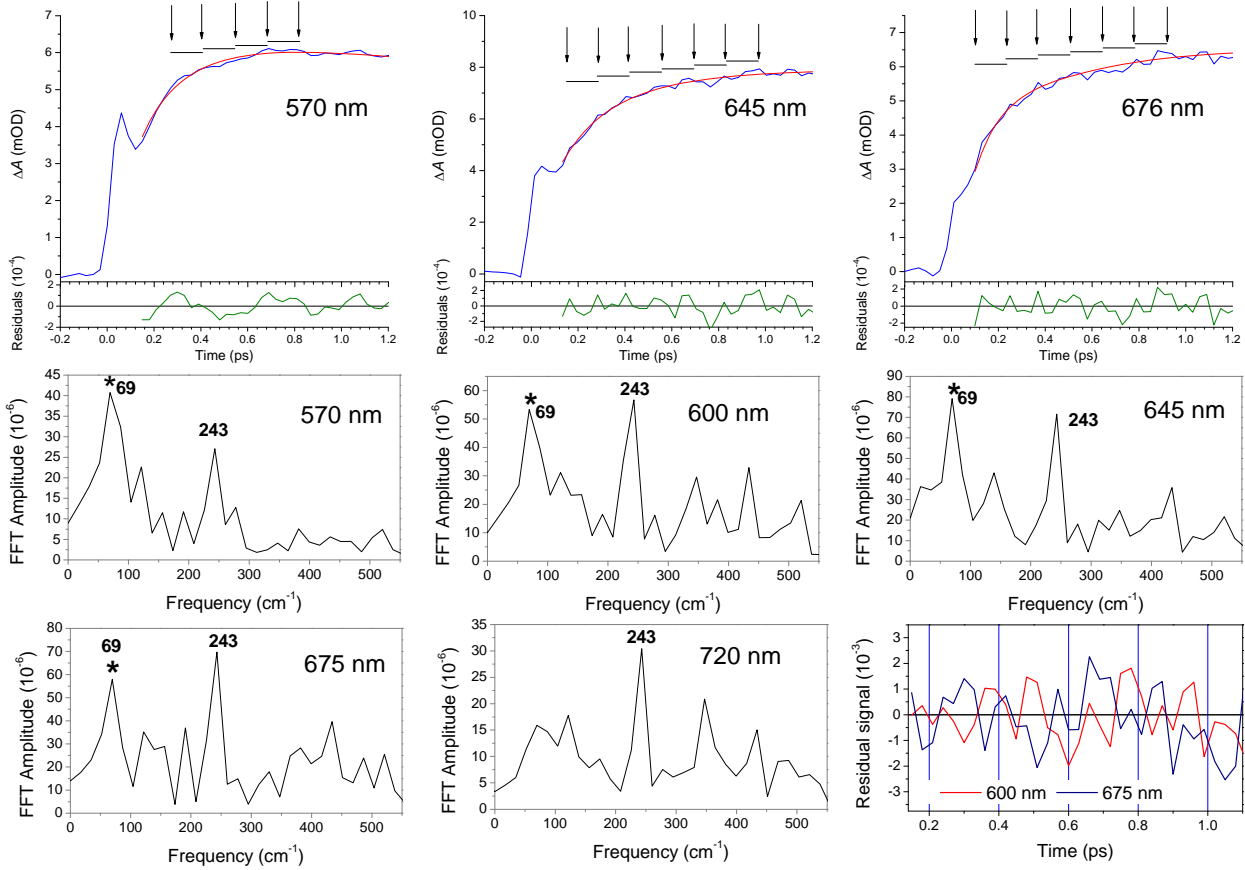


Figure S8. Aqueous IrCl_6^{2-} , 490-nm excitation: the representative short-time 570-, 645- and 676-nm ΔA kinetic traces (blue; solvent contribution subtracted), the multiexponential fits (red) and the fit residuals (green). The horizontal time intervals trace the oscillation maxima of the 243 cm^{-1} Jahn-Teller mode, which has a delayed ($\sim 100 \text{ fs}$) appearance. This mode is further illustrated by FFT spectra of multiexponential fit residuals of the ΔA kinetic traces at several probe wavelengths (570, 600, 645, 675, and 720 nm). Asterisks mark the FFT 69 cm^{-1} signals also observed in transient absorption data measured for the flow cell filled with neat water under the same conditions. The bottom-right panel illustrates the $\sim \pi$ shift (out-of-phase) between the oscillations detected in the blue and red wings (600 and 675 nm) of the 620 nm product transient absorption band, as expected for the oscillations which arise due to vibrational coherence.

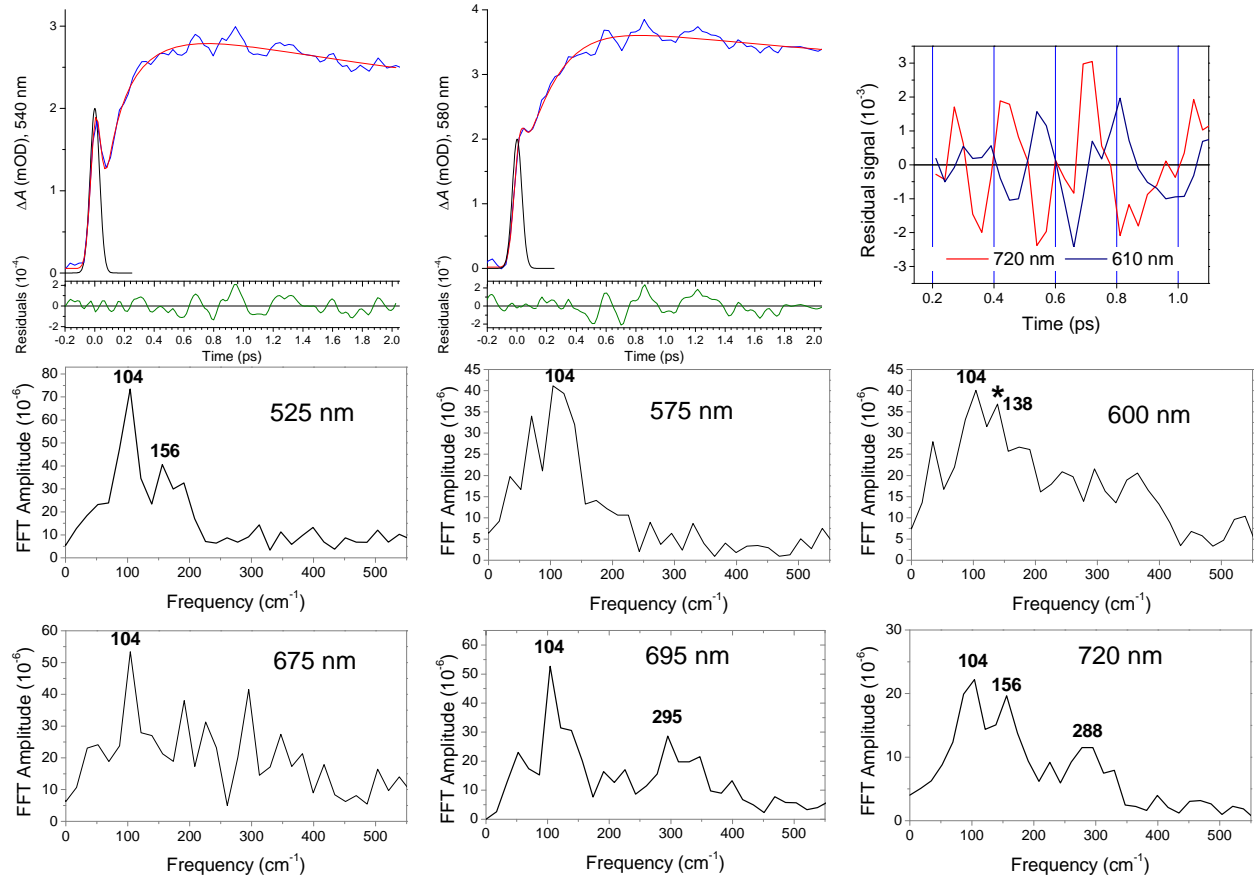


Figure S9. Aqueous IrCl_6^{2-} , 420 nm excitation. Top: the 540- and 580-nm ΔA kinetic traces (blue; solvent subtracted), the multiexponential fits (red) with CCF deconvolution (80 fs CCF fwhm, black), and the fit residuals (green), see also the 525 and 720 nm ΔA data (Fig. 6, main text). The top-right panel illustrates the $\sim\pi$ shift (out-of-phase) between the oscillations detected in the blue and red wings (610 and 720 nm) of the 620 nm ΔA product band, as expected for the oscillations arising due to vibrational coherence. The apparent beat irregularity is caused by the superposition of the water signal at short times and the 156 and 288-295 cm^{-1} ISRS-induced IrCl_6^{2-} ground-state oscillations (bottom-right 720-nm FFT spectrum; IrCl_6^{2-} Raman modes: 160 and 293 cm^{-1} ²). Middle and bottom: FFT spectra of fit residuals of the ΔA kinetic traces are dominated by the Jahn-Teller 104 cm^{-1} mode. An asterisk marks the FFT 138 cm^{-1} signal also observed for the flow cell filled with neat water under the same experimental conditions.

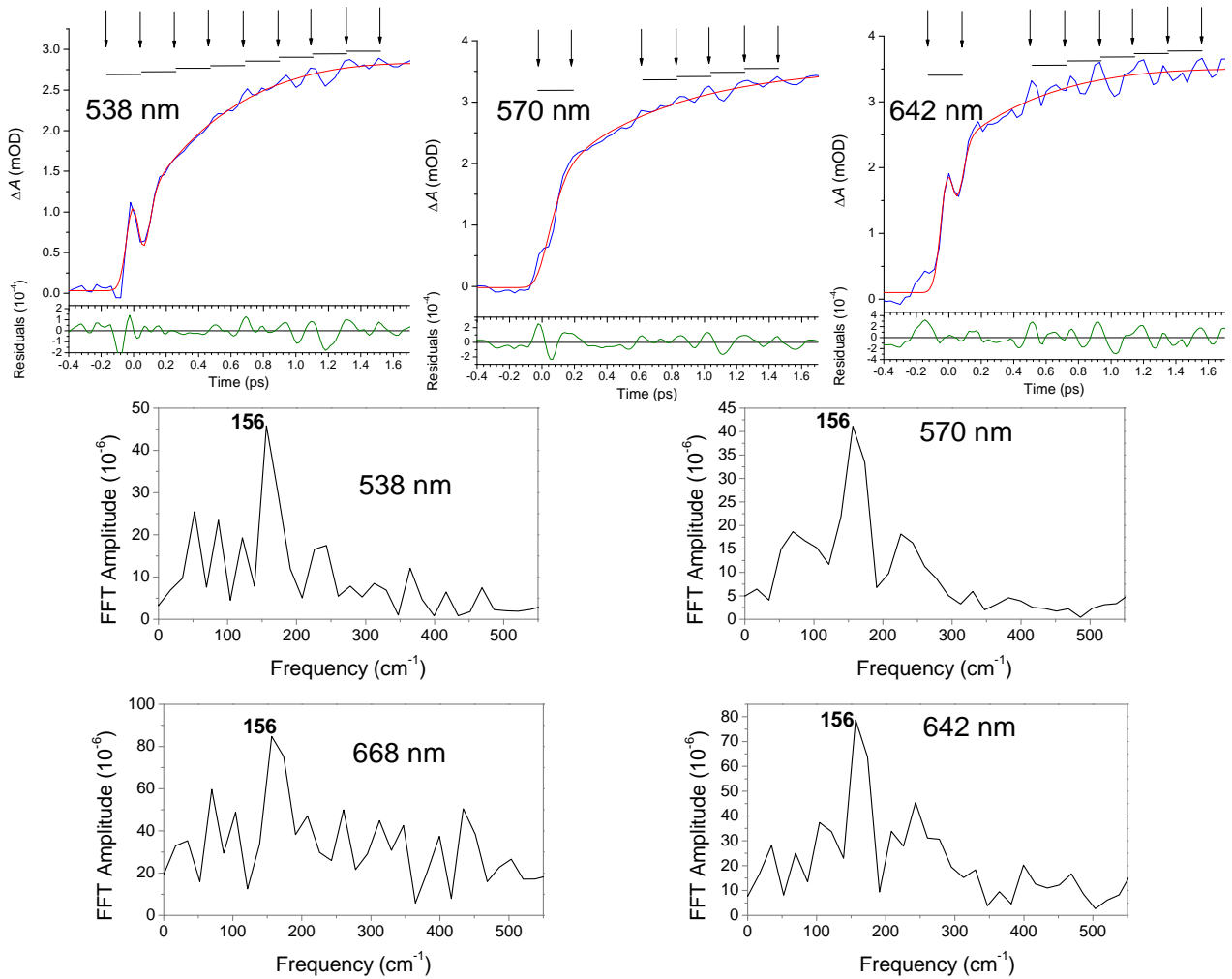


Figure S10. 420 nm excitation of IrCl_6^{2-} in acetonitrile: the short-time 538-, 570- and 642-nm ΔA kinetic traces (solvent contribution subtracted), the multiexponential fits (red) with CCF deconvolution (100 fs fwhm, black), and the fit residuals (green). FFT spectra of fit residuals at several probe wavelengths yield the 156 cm^{-1} band, which frequency matches that of the Raman-active mode of ground-state IrCl_6^{2-} (161 cm^{-1} , acetonitrile¹) and which, therefore, is assigned to ground-state wavepackets excited through ISRS. The horizontal time intervals (top panels) trace the oscillation maxima of the 156 cm^{-1} mode and show that its origin can be traced to the negative delay times, as expected for ISRS oscillations. This 156 cm^{-1} oscillation is observed in addition to the 104 cm^{-1} coherent oscillation due to Jahn-Teller effect, Fig. 6, main text.

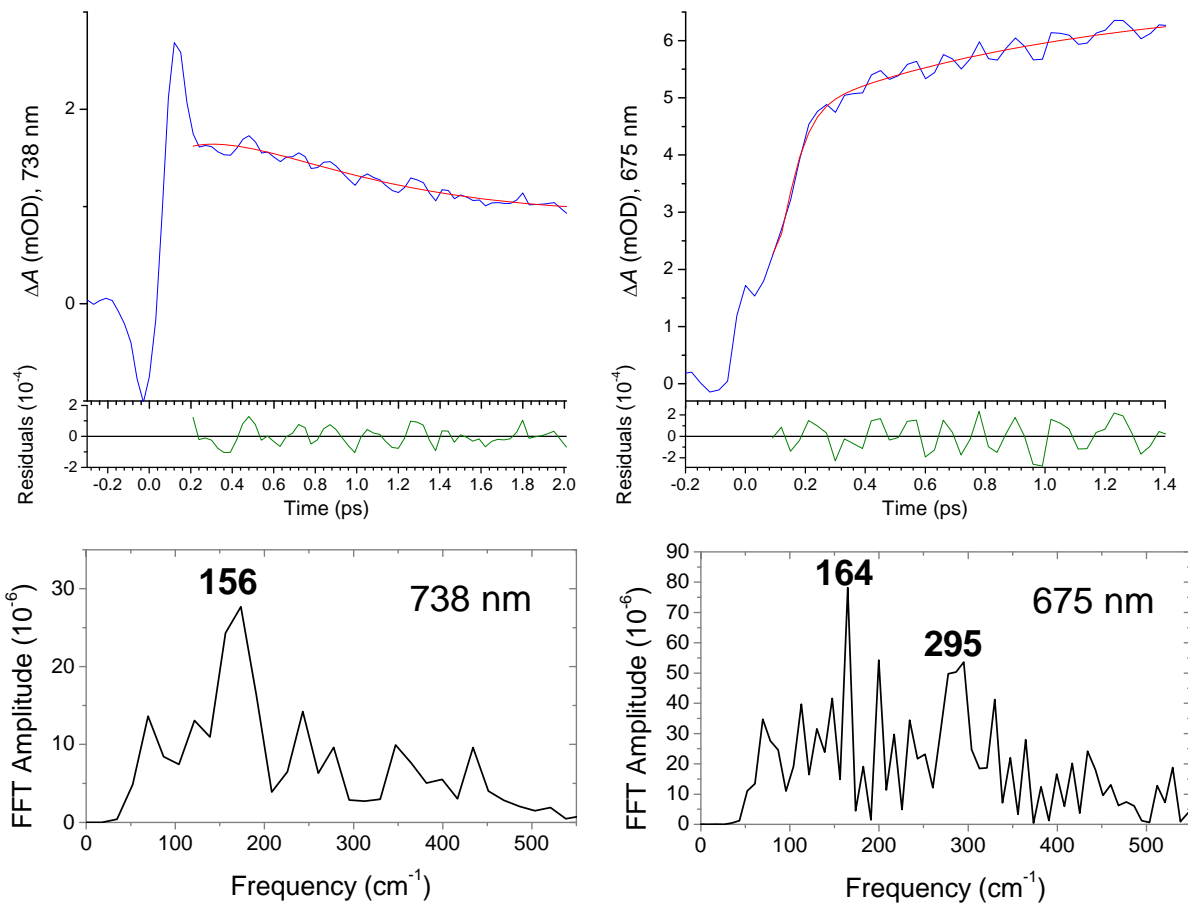


Figure S11. 490-nm excitation of IrCl_6^{2-} in water (left) and acetonitrile (right). The FFT spectra of the multiexponential fit residuals of the 738 nm (left) and 675 nm (right) ΔA kinetic traces (the solvent contribution (present from -100 to 100 fs) not subtracted) show the 156 cm^{-1} and 164 and 295 cm^{-1} bands assigned to ISRS-induced ground-state wavepacket motion (IrCl_6^{2-} Raman modes: 160 and 293 cm^{-1} ^{1,2}, see Table S1). For 490-nm excitation of IrCl_6^{2-} in water, see also Fig. S8.

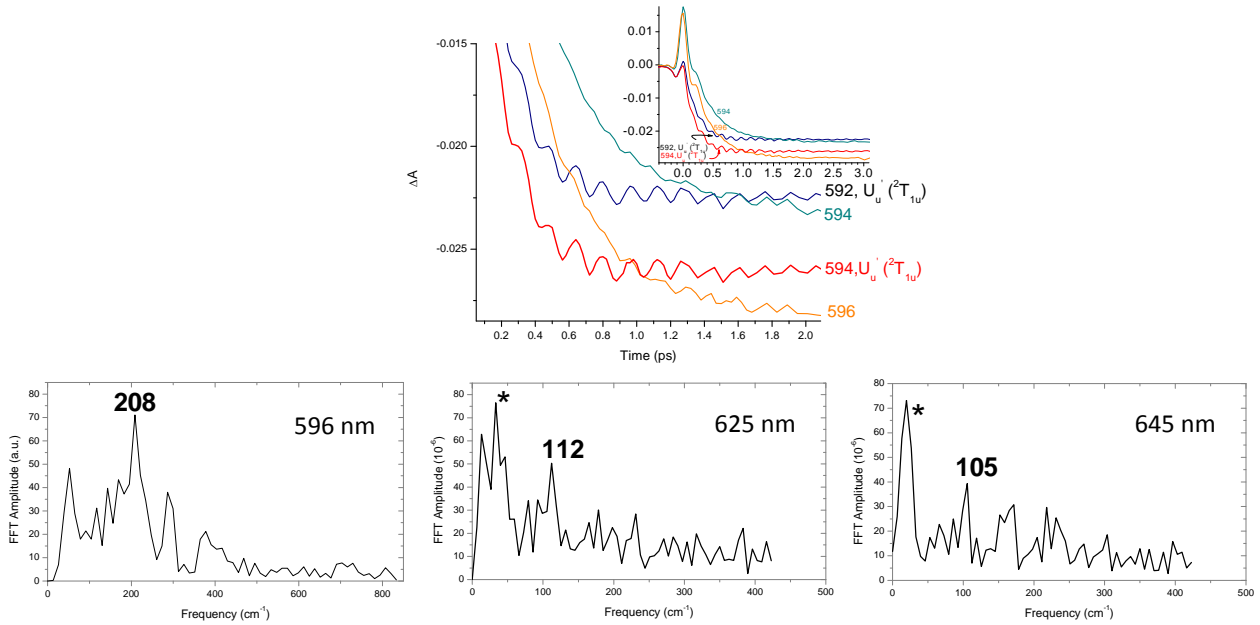


Figure S12. 602-nm $E_u''(^2T_{1u})$ IrBr_6^{2-} excitation in acetonitrile. The 208 cm^{-1} oscillations due to IrBr_6^{2-} ISRS (top, 594- and 596-nm ΔA kinetic traces) are similar to those observed in the previous work³ (top, 592 and 594 nm probe wavelengths, excitation of IrBr_6^{2-} into $U_u'(^2T_{1u})$, see Fig. 10A in ref. [3]; resonance Raman measurements yielded the 208 cm^{-1} mode,^{2,4} see also Table S1.) The FFT spectra of multiexponential fit residuals of the ΔA kinetic traces at several representative probe wavelengths show the 208 cm^{-1} ISRS band and only traces of $104\text{-}121 \text{ cm}^{-1}$ signals, which were intense in the previous work³ upon excitation into $U_u'(^2T_{1u})$, and were attributed to the Jahn-Teller t_{2g} mode.

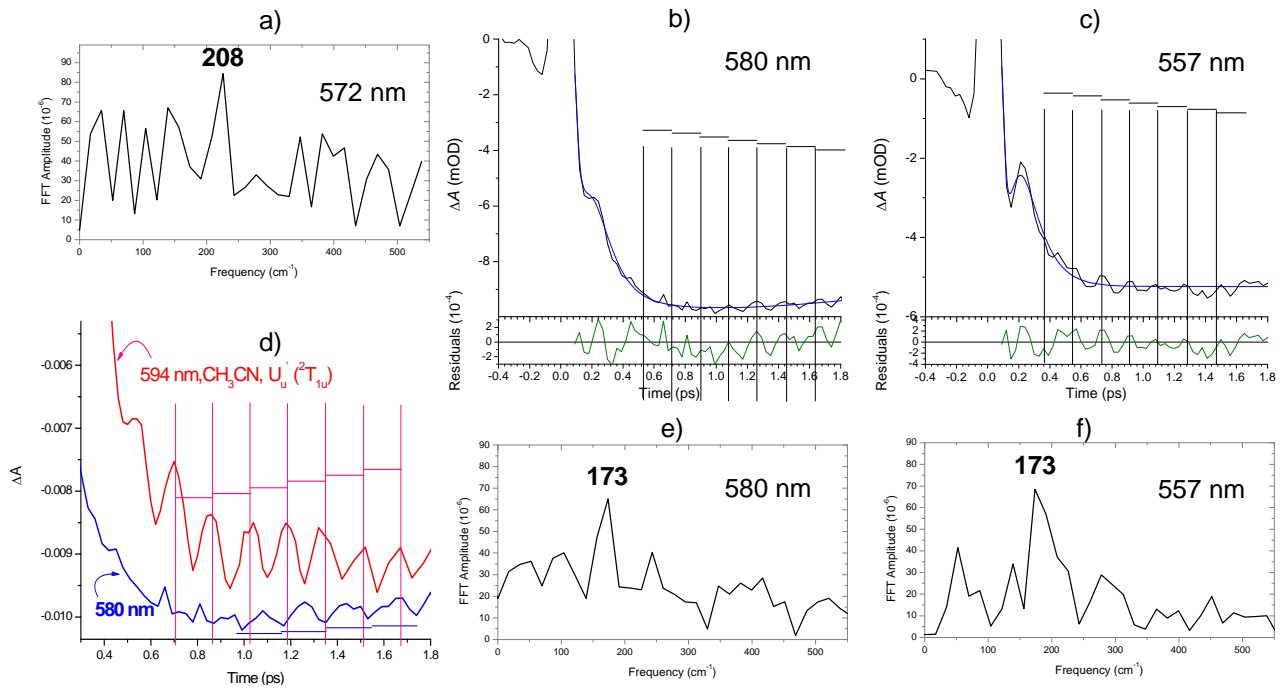


Figure S13. 602-nm $E_u''(^2T_{1u})$ IrBr_6^{2-} excitation in water: the FFT spectra of multiexponential fit

residuals of the ΔA kinetic traces show a 208 cm^{-1} ISRS band (a), similar to acetonitrile solutions in Fig. S12. The comparison of the data in water (d, blue) with $U_u'(^2T_{1u})$ -excited IrBr_6^{2-} in acetonitrile, where the horizontal time intervals (red) trace the oscillation maxima of the 208 cm^{-1} ISRS-induced mode, shows that the oscillations at a smaller frequency are also present. The FFT spectra of the multiexponential fit residuals of the representative 580- and 557 nm ΔA kinetic traces (b and c) show a 173 cm^{-1} band (e and f), which frequency matches the 174 cm^{-1} Raman mode of aqueous IrBr_6^{2-} ^{2,4} and which, therefore, is assigned to ground-state wavepacket induced through ISRS. Oscillations at smaller frequencies (e.g., 125 cm^{-1} Jahn-Teller mode, ref. [3]) were not detected. In windows b) and c), the horizontal time intervals trace the oscillation maxima of the 173 cm^{-1} ISRS mode.

Table S1. Vibrational frequencies of IrCl_6^{2-} and IrBr_6^{2-} observed in the current work and reported in literature.

	Frequencies (cm^{-1}) acetonitrile solution		Frequencies (cm^{-1}) aqueous solution	
IrCl_6^{2-}	This work	Known Raman modes from literature	This work (cm^{-1})	Known Raman modes from literature
600 nm	350 ^c	161, 290, 341 ^b	156, 287 ^c	160, 293, 345 ^a
490 nm	164, 295 ^c		156, 295 ^c 243 ^d	
420 nm	156 ^c		156, 295 ^c 104 ^d	
IrBr_6^{2-}				
602 nm	208 ^c ^f	208 ^e	173, 208 ^f	97, 174, 210 ^a 97, 177, 212 ^g

^a Ref. [2]. ^b Ref [1]. ^c Assigned to ISRS-excited ground-state modes. ^d Assigned to Jahn-Teller modes (t_{2g} -like, 104 cm^{-1} ; e_g -like, 243 cm^{-1}). ^e Ref. [3]. ^f 104 cm^{-1} oscillations in acetonitrile and 125 cm^{-1} oscillations in aqueous solutions assigned to the Jahn-Teller t_{2g} -like mode; excitation into $\text{U}_u(^2\text{T}_{1u})$ and $\text{U}_u(^2\text{T}_{2u})$ states, ref. [3]. ^g Ref. [4]

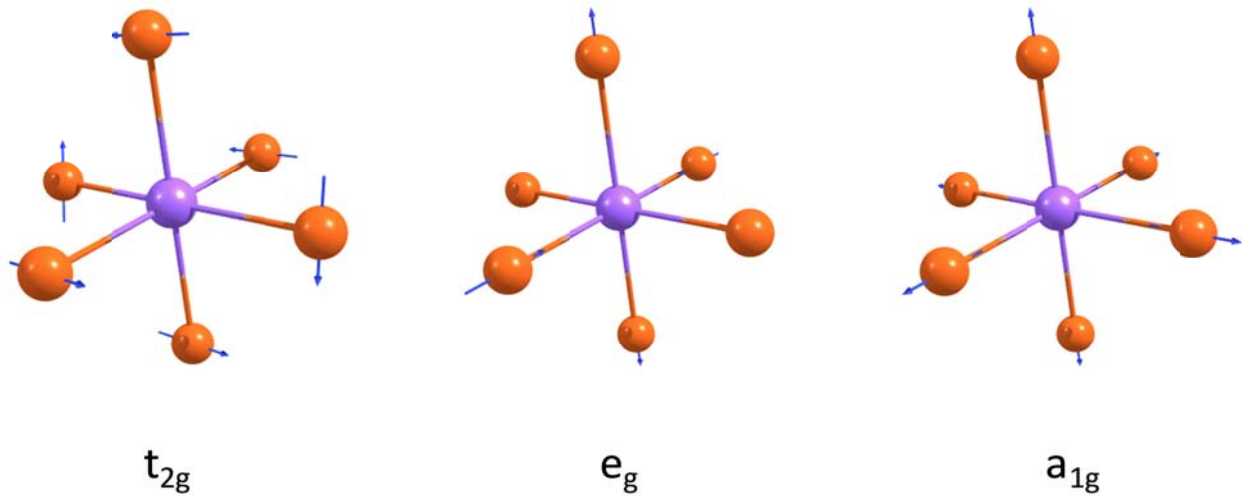


Figure S14. Nuclear motion in IrCl_6^{2-} and IrBr_6^{2-} octahedral complexes corresponding to Raman- and Jahn-Teller-active t_{2g} bending (triply degenerate), e_g out-of-phase stretching (doubly degenerate), and a_{1g} totally symmetric stretching modes.

References

1. H. Hamaguchi and T. Shimanouchi, *Chem. Phys. Lett.*, 1975, **32**, 103.
2. Y. M. Bosworth and R. J. H. Clark, *J. Chem. Soc. Dalton Trans.*, 1974, **5**, 1749.
3. S. M. Matveev, D. S. Budkina, I. L. Zheldakov, M. R. Phelan, C. M. Hicks and A. N. Tarnovsky, *J. Chem. Phys.*, 2019, **150**, 054302.
4. H. Hamaguchi and T. Shimanouchi, *Chem. Phys. Lett.*, 1976, **38**, 370.